International Journal of Rock Mechanics & Mining Sciences 61 (2013) 196–211

Contents lists available at SciVerse ScienceDirect

International Journal of Rock Mechanics & Mining Sciences

journal homepage: www.elsevier.com/locate/ijrmms

Thermally vs. seismically induced block displacements in Masada rock slopes

Dagan Bakun-Mazor [a], Yossef H. Hatzor [a,*], Steven D. Glaser [b], J. Carlos Santamarina [c]

[a] Department of Geological and Environmental Sciences, Ben-Gurion University of the Negev, Beer-Sheva 84105, Israel
[b] Department of Civil and Environmental Engineering, University of California Berkeley, Berkeley, CA 94720-1758, USA
[c] School of Civil and Environmental Engineering, Georgia Institute of Technology, Atlanta, GA 30332-0355, USA

ARTICLE INFO

Article history:
Received 21 June 2012
Received in revised form
6 February 2013
Accepted 5 March 2013

Keywords:
Rock slopes
Slope stability
Thermo-elasticity
Thermally-induced sliding
Earthquakes
Site response

ABSTRACT

We compare thermally and seismically induced sliding mechanisms of blocks that are separated from the rock mass by a tension crack and slide along a frictional interface. The rock slopes of Masada Mountain, Israel, are used to demonstrate our approach. Crack displacement coupled with thermal fluctuations is measured in the West slope of the mountain during two years (2009–11). Physical and mechanical lab tests provide the assumed depth of penetration of the heating front during seasonal cycles of exposure as well as the thermal expansion coefficient of the rock mass. These, along with the shear stiffness of the sliding interface, allow us to quantify the expected thermally induced displacement rate of blocks in Masada, through a proposed wedging–ratcheting failure mechanism. A distinct block in the East slope of the mountain exhibiting a tension crack opening of 200 mm was monitored for displacement and temperature during a single seasonal cycle in 1998. Based on the assumed seismicity of the region and the known topographic site effect, along with the laboratory measured frictional resistance and shear stiffness of the sliding interface, we subject the mapped geometry of the block in the East face to simulated cycles of earthquake vibrations utilizing the numerical, discrete element, discontinuous deformation analysis (DDA) method. We find that for a time window of 5000 years, the observed 200 mm displacement of the East slope block is more likely to have been thermally, rather than seismically, controlled. This result implies that in climatic regions where the temperature amplitude over a seasonal cycle is sufficiently high, thermally induced displacements play an important role in rock slope erosion.

1. Introduction

Various environmentally induced mechanisms have been considered in an attempt to explain slope failures in rock masses along pre-existing discontinuities. High-magnitude earthquakes e.g. [1,2], pore pressure buildup in rock joints e.g. [3,4], and freezing and thawing of water in joints e.g. [5–7] have been suggested as trigger factors for landslides and rock avalanches. These suggested mechanisms fail to describe time-dependent, thermally controlled, sliding along discontinuities or opening of tensile fractures which may ultimately culminate in slope failure.

1.1. Thermal considerations in rock slope stability

Considering daily and seasonal temperature influences, many researchers have detected extremely slow, creep-like, slope displacements due to cyclic temperature changes in long-term monitoring surveys [8–13]. The motivation for some of these monitoring surveys was the preservation of cultural heritage sites around the world, for example in Slovakia [14], Japan [15], and Israel [16].

Gunzburger et al. [10], in their investigation of the Rochers de Valabres slope in the Southern Alps of France, found that daily surface temperature oscillations played an important preparatory role in rock fall events using a high-precision geodetic monitoring system and numerical modeling. They showed that daily temperature fluctuations may be responsible for generating irreversible displacements on some fractures. Nevertheless, they concluded that the monitoring of preparatory factors was not sufficient to predict eminent slope collapse. Mufundirwa et al. [12] monitored natural rock slope deformation due to thermal stresses across fractures in a chert rock mass. By a new method to minimize displacement proportional to temperature, they recovered the recognized displacement that has been related to reversible thermo-elastic response of the rock mass and the sensor and concluded that thermal fatigue predominantly caused permanent fracture deformations. Gischig et al. [8,9] demonstrated how thermo-mechanical effects can drive rock slope deformation at greater depths below the annual thermally active layer. They found that deformation and progressive rock slope failure can be driven solely by thermo-mechanical forcing.

Various researchers have suggested that daily and seasonal temperature fluctuations may generate thermally induced stresses sufficiently high to propagate pre-existing cracks in the rock mass [17]. Although the seasonal temperature front penetrates only

* Corresponding author. Tel.: +972 8 6472621; fax: +972 8 6248717.
E-mail address: hatzor@bgu.ac.il (Y.H. Hatzor).

1365-1609/$ - see front matter © 2013 Elsevier Ltd. All rights reserved.
http://dx.doi.org/10.1016/j.ijrmms.2013.03.005

a few meters into the rock mass, it may still have significant mechanical consequences in terms of displacements or stress changes far from the rock surface, especially for rock slopes with critically stressed discontinuities e.g. [8–10].

Watson et al. [13] utilized data obtained from an extensive instrumentation monitoring program at the Checkerboard Creek in British Columbia, Canada. Their monitoring record indicates a persistent annual displacement cycle that matches the thermal cycle, as recorded near the bedrock surface. Their numerical analysis indicates that the permanent displacement occurs along steeply dipping discontinuities which often intersect in the rock mass to form wedges. They showed that the thermal displacement occurs in response to reduction in effective stress during the cooling season.

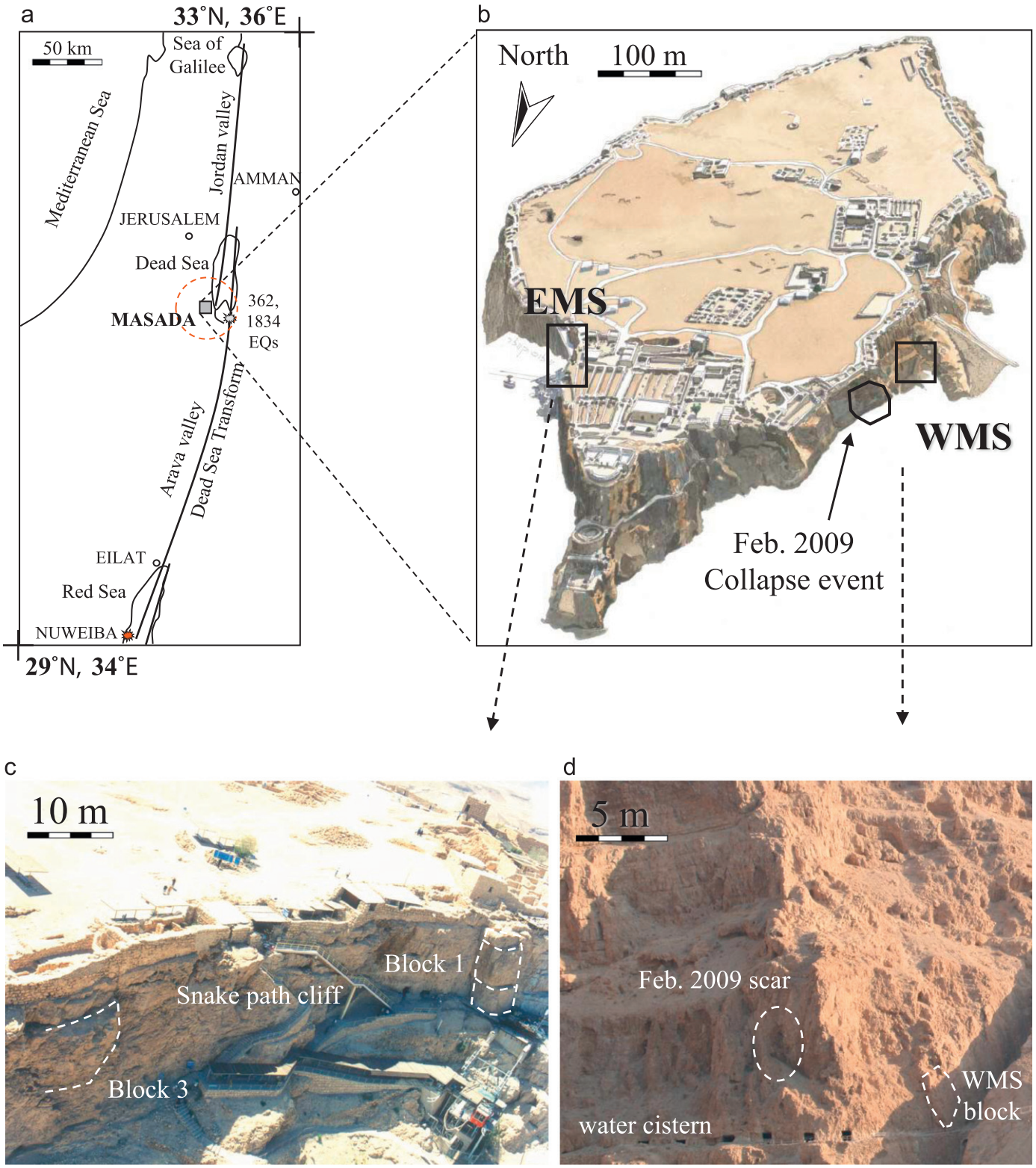

Fig. 1. Location maps: (a) Masada Mountain in the Western margins of the Dead Sea rift valley, (b) location of the monitoring stations (EMS=East Masada Station; WMS=West Masada Station), (c) monitored blocks in the "Snake Path" cliff (EMS), (d) collapsed block at WMS.

1.2. Seismic considerations in rock slope stability

While observations and models for thermally-induced rock block displacements are relatively new, various methods have been developed over the last century to consider seismic induced displacement in rock slope stability. A pseudo-static limit equilibrium analysis is available, provided that the slip surface geometry and available shear strength along the sliding surface are known e.g. [18,19]. Alternatively, a dynamic analysis for rigid block sliding on a single plane was suggested both by Newmark [20] as well as Goodman and Seed [21]. This procedure, largely known as "Newmark type analysis", assumes that permanent deformation initiates when earthquake-induced inertial forces acting on a potential sliding block exceed the yield resistance of a slip surface. More recently, with the advent of numerical tools, it has become possible to apply a fully dynamic analysis for discontinuous media using discrete element methods [22,23]. The advantage of the numerical approach is the ability to model complex block geometries and the fact that the mode of failure is a result, not an assumption, of the analysis.

Considering steeply dipping slopes, macro-seismic observations have shown that the effects of local topography on ground motion might be of great importance, as variations both in the amplitude and the frequency content across the mountain slopes have been reported. Topographic amplification is frequency dependent and reaches a maximum at the resonance frequency of the mountain. This effect is more pronounced in the horizontal, rather than the vertical component, where typically the preferential direction is perpendicular to the mountain axis e.g. [24,25–28].

1.3. Comparison between thermally vs. seismically induced displacement using the Masada slopes as case study

In this paper we suggest a thermally induced wedging mechanism that explains how cyclic thermal oscillations induce intermittent expansion and contraction of the tension crack, causing seasonal translation of rock blocks. We present new evidence for thermally induced block displacements using both thermal and displacement data from a monitored rock block in the West face of Masada Mountain, Israel, along with re-visited and re-analyzed monitoring data from the East face of Masada. A removable block at the Eastern slope of the mountain, referred to as Block 1, is used as a case study, where an accumulated displacement of 200 mm took place during the geological history. The theoretical possibility of obtaining thermally induced block displacements in Masada rock slopes is explored, given the measured seasonal temperature amplitude and the mechanical and physical properties of the rock mass. We then address seismic loading in Masada rock slopes based on the assumed seismicity of the region and the measured topographic site effect in the mountain. The two loading mechanisms, thermal vs. seismic, that drive rock slope deformation are discussed and their relative significance in rock slope deterioration are compared.

1.4. Geological setting of Masada

Masada Mountain, a world heritage site, is an uplifted horst within the band of normal faults that comprise the western margins of the Dead Sea rift valley (see Fig. 1a). The rock mass consists of bedded dolomites and limestones, inclined 5° up to 20° to the East (J1), and is intensely fractured by two orthogonal, sub-vertical, and very persistent joint sets, striking roughly parallel and normal to the long axis of the mountain, where J2 set strikes NNE and J3 strikes ESE. In a regional study in the western margins of the Dead Sea pull-apart, Sagy et al. [29] suggest that these two dominating regional joint set patterns were developed during a single tectonic phase. The mean joint spacing at Masada varies from few decimeters in the West face and up to 5–10 m in the East face of the mountain [11].

1.5. Climatic setting and observed weather induced collapse in Masada

Climatically, Masada Mountain is located in the Eastern part of the Judean Desert, an arid zone with mean annual rainfall values of 35 mm/year, and average seasonal minimal and maximal temperatures of 12.7 °C and 39.7 °C, respectively, as reported by the Israeli Meteorological Service [30] for the period of 1983–2000. Within the framework of the MASAL research project (Meteorological Observation and Assimilation of the Atmosphere on Long term, Dead Sea, Israel) [31,32] a fully equipped meteorological station, located 300 m from the West slope of Masada, has been recording the amount of precipitation, temperature, and wind velocity since 2006.

During the night of February 10, 2009, a heavy rain storm struck the West face of Masada Mountain. Consequently, a sizeable rock fall was triggered, the debris of which damaged the ancient path leading to the water cisterns that were excavated by the Romans some 2000 years ago for water storage in the Western cliffs of the mountain. The February 10, 2009, slope failure (Fig. 1d) was the motivation for installing a monitoring system in the West slope of the mountain by us in July 2009, for investigation of the dynamic response of rock blocks to thermal fluctuations.

2. West and east monitoring stations in Masada

2.1. West Masada station (WMS)

In order to measure with high precision the rock block response to daily and seasonal environmental oscillations, a monitoring system was installed in June 2009 on a single block separated from the West cliff of Masada by two intersecting joint sets (Fig. 2). The monitoring system, manufactured by SIM STRUMENTI SNC [33], consisting of four joint meters, temperature, and relative humidity transducers, has been collecting output data at an acquisition rate of 12 samples per day since July, 2009. The layout of the joint meters as installed in the Masada West Station (WMS) is presented in Fig. 2.

The joint meters (model DS810) are 50-mm-range Potentiometers with measurement accuracy of +/−0.02 mm. The thermal expansion coefficient of the joint meter is $1.5\times10^{-6}/^{\circ}C$ and its calibrated operating range from −30 °C to +100 °C. The static end of each joint meter containing the sensor was anchored to the massive rock body while the free end was attached to the removable block. The joint meters (WJM 1–4) were installed perpendicular to the joint trace as follows: WJM 1 was installed on an open joint belonging to joint set J2, WJM 2 and WJM 3 were installed across a joint belonging to joint set J3. In order to account for thermal effects on the monitoring system a dummy joint meter (WJM 4) was installed directly on the intact, continuous rock face. Details for joints openings and joint meters configuration are given in Table 1.

Air temperature was measured by a temperature sensor (model WE710) with precision of 0.25 °C and a range from −25 °C to 105 °C. Relative humidity was measured by a humidity meter (model WE720) under an operating temperature range from −20 °C to +80 °C. The measurement devices were connected to two separate data acquisition systems (Model ML-4CH).

2.2. East Masada station (EMS)

In a previous study Hatzor [11] monitored time dependent displacements of rock blocks (referred to as "Block 1" and "Block3" in that study) embedded in the "Snake Path" cliff of the East face of Masada Mountain (Fig. 1c), using joint meters. Block 1 is a

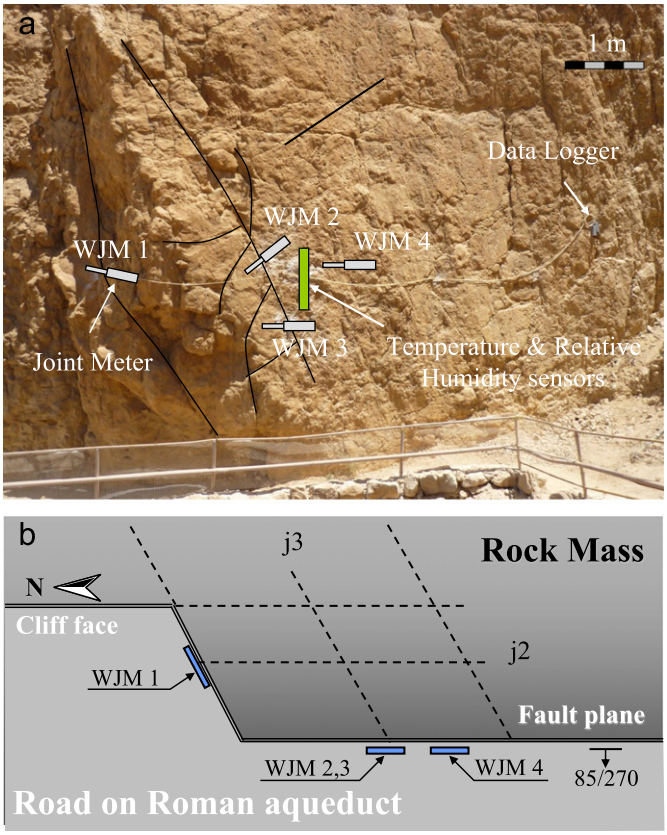

Fig. 2. The environmental monitoring system at WMS: (a) Face view of monitored block (WJM=West Joint Meter), and (b) plan view schematically illustrating the rock mass structure and joint meter position. For joint and joint meter data see Table 1.

Table 1
Joint Meters (*JM*) configuration in the Masada West slope monitoring station (WMS).

JM	Distance between bolts (cm)	Joint opening (cm)	JM orientation (dip/dip direction)
1	26.4	10–12	2/250
2	25.2	3–12	33/340
3	25.0	1	3/180
4	24.8	–	0/000

prismatic block resting on a gently (19 °C) Easterly-dipping bedding plane (J1), separated from the cliff by two sub-vertical, orthogonal tension cracks (J2 and J3) (see Fig. 3a). The block height is 15 m and its width is about 7 m. Four joint meters (EJM 1–4) were mounted across the two tension cracks that separate Block 1 from the "Snake Path" cliff, along with a temperature transducer (T1) that was mounted inside an open tension crack at the back of the block (see Fig. 3a). Block 3, located on the south part of the cliff (see Fig. 1c), separated from the rock mass by a single tension crack, also rests on an Easterly dipping bedding plane. Two joint meters (EJM 10 and 11) were installed across the tension crack (J3) at the back of the block. Another temperature transducer (T2) was installed within an open fracture near the block (Fig. 3b).

Time–dependent displacements of Block 1 and Block 3 and the air temperature near the blocks were recorded from January 14 to June 30, 1998. A cable bolt anchoring system was then installed in Block 1 in connection with a slope reinforcement campaign that was conducted at the East slope at that time, while Block 3 remained unsupported. The East slope monitoring system of Hatzor [11] is referred to here as "Masada East Station" (EMS).

3. Temperature and displacement monitoring results

The outputs of WMS instruments are plotted in Fig. 4 for a period of 25 months (July 2009–August 2011). The joint meters were wired such that joint opening returns positive output. The raw data recorded at 2 h intervals is shown in Fig. 4a (gray lines), smoothed by daily moving average (solid lines). As clearly indicated in Fig. 4a the "dummy" joint meter installed on intact bedrock (WJM 4) shows a nearly static response while the rock joints (WJM 1–3) exhibit relatively large fluctuations over time. To study the relationship between air temperature and joint displacement, moving averages with a 30 day time window has been performed on the original raw data obtained from WJM 1–4. The results are plotted in Fig. 4b as a function of time, and an inverse relationship between cooling and joint closure is clearly indicated. Note that the output of dummy transducer (WJM4) exhibits a certain amount of drift, believed to be an artifact as the transducer is mounted on solid rock.

Results obtained from Blocks 1 and 3 at EMS are shown in Fig. 5 for a period of 5.5 months between January 14 and June 30, 1998. Since the data acquisition rate in EMS was not constant, Fig. 5

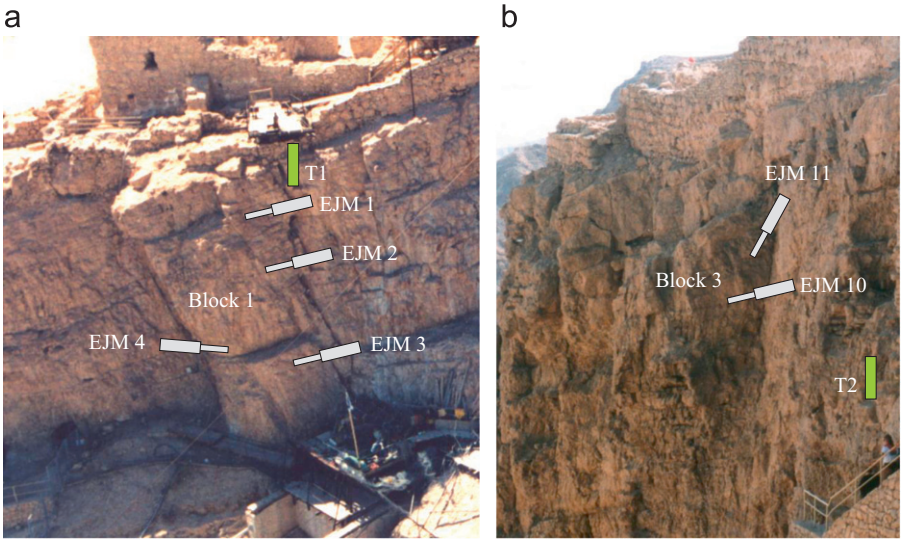

Fig. 3. Monitoring system layout at EMS [after 11] where EJM stands for East Joint Meter: (a) Block 1 and (b) Block 3.

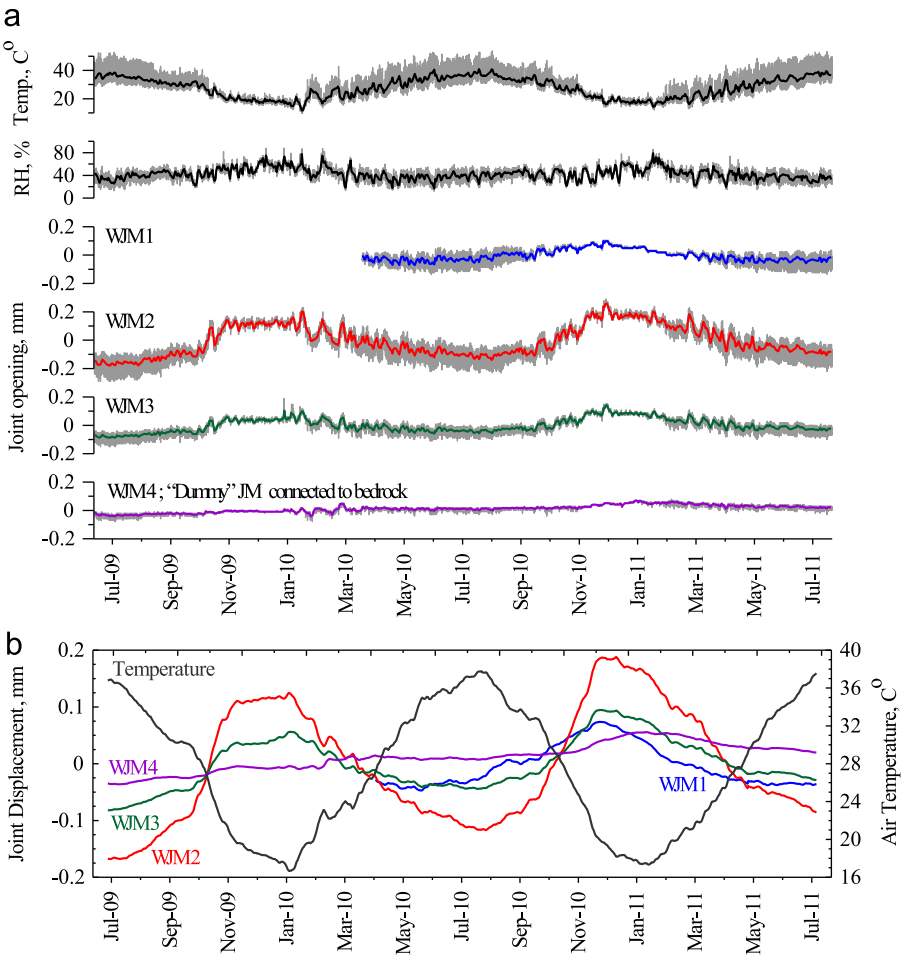

Fig. 4. WMS output from July 2009 to August 2011 (Joint opening is positive): (a) original data sampled every 2 h (gray lines) smoothed by daily moving average (solid), (b) temperature and joint displacement vs. time using monthly moving average.

represents the joint meter displacement (in mm) and air temperature as a function of time, using daily average data. The joint meters output was zeroed such that the beginning of the monitoring period was set at the origin for each joint meter output. Accumulated joint closure related to increasing air temperature was recorded at all joint meters during the monitoring period at the East slope. Although a full annual period was not recorded in EMS during the monitoring survey at 1998, it is clearly evident that inter-seasonal fluctuations in air temperature directly affect joint opening and closing, as inferred from the joint meters output.

In contrast to the short monitoring period in East slope, the recent monitoring data from the West slope provide information about long-term joint displacement and air temperature and the relationship between them. The annual amplitude of both air temperature and joint displacement can be inferred from the results. The annual amplitude recorded by WJM 2 is 0.14 mm while the annual air temperature amplitude is 9.1 °C.

Monitoring data presented in Figs. 4 and 5 from WMS and EMS suggest that joint opening and closure are strongly correlated with air cooling and heating. This correlation implies that contraction and expansion of the rock on both sides of the crack manifests in joint opening or closure, as clearly indicated by joint meter outputs. The relationship between joint opening and air temperature for one annual cycle in WMS is plotted in Fig. 6 using monthly averaging of the raw data. The annual cycle for WJM 1 begins on May, 2010 and ends on May 2011; the annual cycle for WJM 2, 3, and 4 is from August 2009 to August 2010. To demonstrate the time dependent path of the monitored joint displacement, the beginning and end of the annual cycle are denoted in the figure.

An inverse relationship between joint opening and air temperature is obtained with a relatively high linear correlation for WJM 2 and 3 (Fig. 6), implying that the dominant factor affecting joint displacement is thermo-elastic, the majority of which is recovered by the end of an annual loading cycle (Fig. 6a). In order to address the drift of WJM 4, and assuming that all joint meters have a similar drift, we subtract the output of WJM 4 from the output of WJM 1, 2, and 3 and show the results in Fig. 6b. The subtraction of WJM 4 data suggests that at the end of an annual cycle the monitored joints do not exhibit any permanent deformation.

4. Thermally induced block displacements

In this section we explore the possibility of obtaining thermally induced block displacements in Masada rock slopes, given the measured seasonal temperature amplitude and the mechanical and physical properties of the rock mass.

A conceptual model of thermally induced block sliding is schematically illustrated in Fig. 7 following original ideas presented by Watson et al. [13]. With seasonal cooling the sliding block contracts, as a response the tension crack opens, and the wedge block penetrates into the newly formed opening in the tension crack. In summer, when the temperature rises, the sliding block expands and the wedge block is locked in place, prompting compressive stress generation in the block system and pushing the

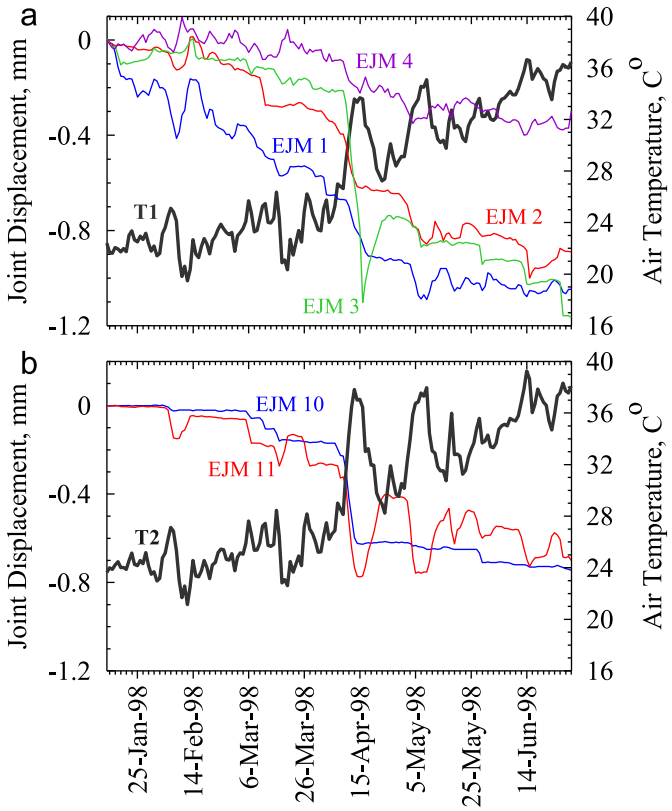

Fig. 5. EMS output data from January 14 to June 30, 1998 (Joint opening is positive, T=temperature transducer). (a) Block 1 and (b) Block 3.

sliding block down slope. In the next cooling season shrinking of the sliding block enables further penetration of the wedge into the tension crack, and consequently further down slope block displacement commences in the summer by shear sliding along the sliding surface.

Gunzburger et al. [10] argue that thermo-mechanical creep may take place without necessarily having a wedge in the tension crack, for instance when the sliding bock is located in a critical state from a mechanical point of view, namely very close to its limiting equilibrium. In the wedging mechanism, however, the block can slide downward even if it rests on gently dipping sliding surfaces, as will be shown later. Moreover, the wedging fragments are required in cases where the rock underlying the sliding plane also undergoes thermally induced expansion and contraction at the same rate and amount as the sliding block. In such a case, only a continuous supply of rock fragments into the opening tension crack will enable compressive stresses to develop and will prevent closure of the tension crack, thus allowing progressive down plane displacement. A similar wedging process has been suggested for fluvial erosion of river bedrock by plucking of loosened blocks [34].

A recent photograph of Block 1 in EMS is shown in Fig. 8, where the old EJM 1 and 2 that were installed in 1998 are still visible today. Inspection of the photograph reveals that the block has clearly separated from the cliff over the historic time by accumulated displacement of about 200 mm, and that sizeable rock fragments fill the aperture of the tension crack. It is suggested here that these rock fragments can play the role of the wedge block in a thermally induced wedging mechanism. In order to test the applicability of a thermally induced wedging mechanism for the observed displacement of Block 1 in Masada, we utilize here an analytical approach suggested by Pasten [35]. For input data we use the temperature and displacement monitoring results from the West slope (Fig. 4), along with laboratory tests for determining the thermal and mechanical properties of the Masada rock mass.

4.1. Theoretical considerations

Consider the exact geometry of Block 1 as shown in Fig. 9. The tension crack of length L_W is filled with rock fragments that represent the wedge block shown in the conceptual model in Fig. 7 and the actual rock fragments captured in the photograph in Fig. 8. The length and height of the sliding block are L_B and H, respectively. We assume here that the rock block is a homogeneous slab experiencing a change of temperature in its center from an initial temperature T_o to a new boundary temperature T_1. The homogenization time t^* required for the block center temperature to reach 99% of the new boundary temperature T_1 can be estimated as $t^*=2L^2/D_T$, where L is the slab length and D_T is the thermal diffusivity of the rock which is proportional to the rock thermal conductivity (λ), and inversely proportional to its mass density (ρ) and specific heat capacity (C_p) [36]. Following Pasten [35], the depth of penetration of the heating front during an annual cycle, referred to here as the "thermal skin depth" (S_d), may be estimated as

$$S_d \approx \sqrt{\frac{\lambda t_{\exp}}{2\rho C_p}} \quad (1)$$

where t_{exp} is the exposure time for the given period of interest, assuming it is shorter than the homogenization time ($t_{exp} < 2L^2/D_T$). If $t_{exp} > 2L^2/D_T$ then $S_d = L/2$. For a single seasonal cycle we assume $t_{exp} \approx 180$ days.

Given the physical properties of the Masada rock mass (see next section), the estimated thermal skin depth for Block 1 is wider than the wedge length L_W but smaller than the block length L_B, as shown schematically in Fig. 9.

Pasten [35] suggests three displacement components that are involved in the thermal expansion process: the thermal expansion (δ_T), the elastic compression of the rock material (δ_σ), and the

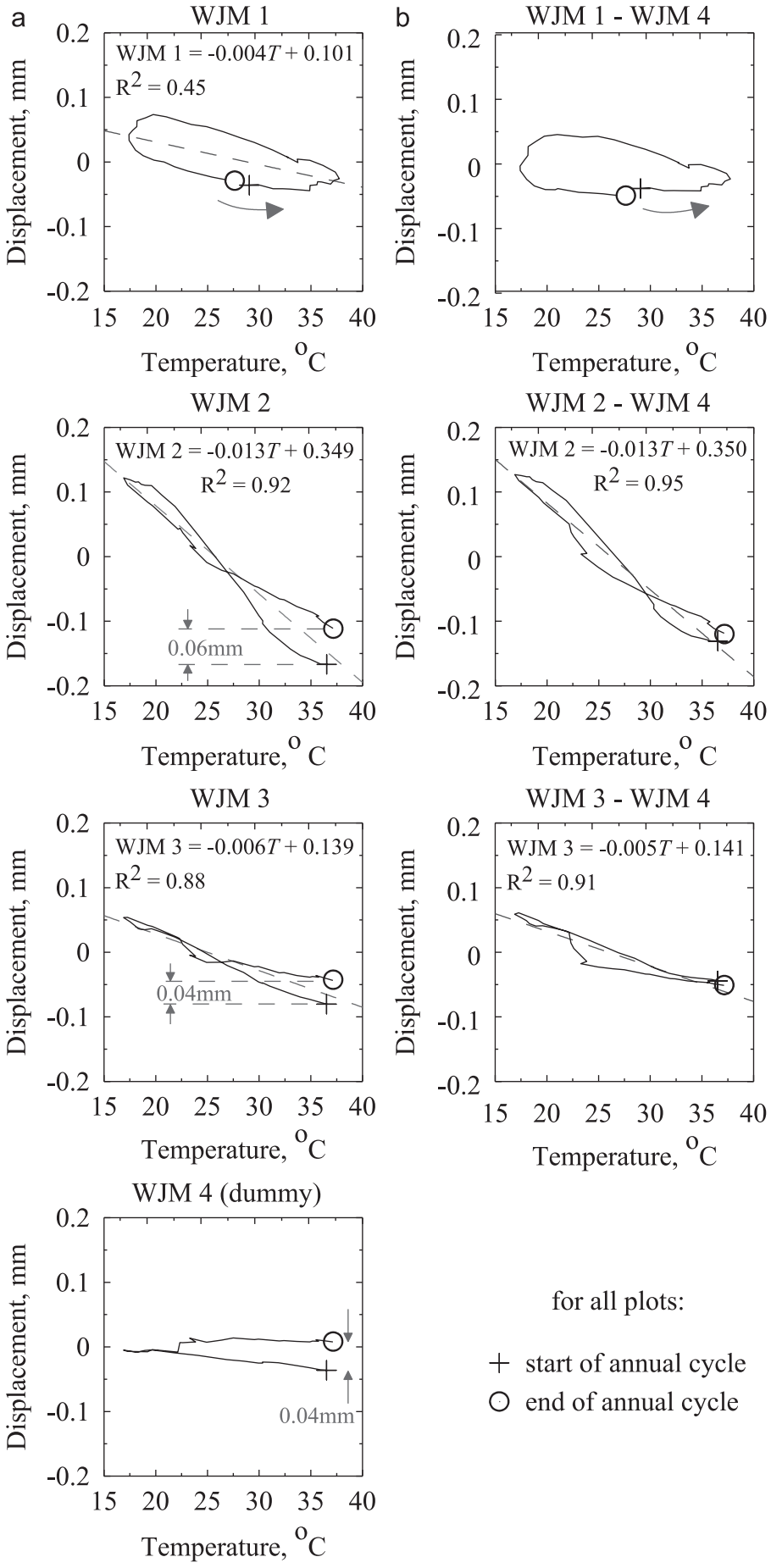

Fig. 6. Joint opening vs. air temperature smoothed by monthly averaging for one annual cycle (Joint opening is positive): (a) smoothed data with no correction where accumulated annual displacement is denoted, and (b) WJM 1,2,3 corrected for apparent temperature effect as obtained from dummy transducer WJM 4. WJM 1 from May 2010 to May 2011, WJM 2, 3, 4 from August 2009 to August 2010. Best fit linear curves are shown as dashed gray lines.

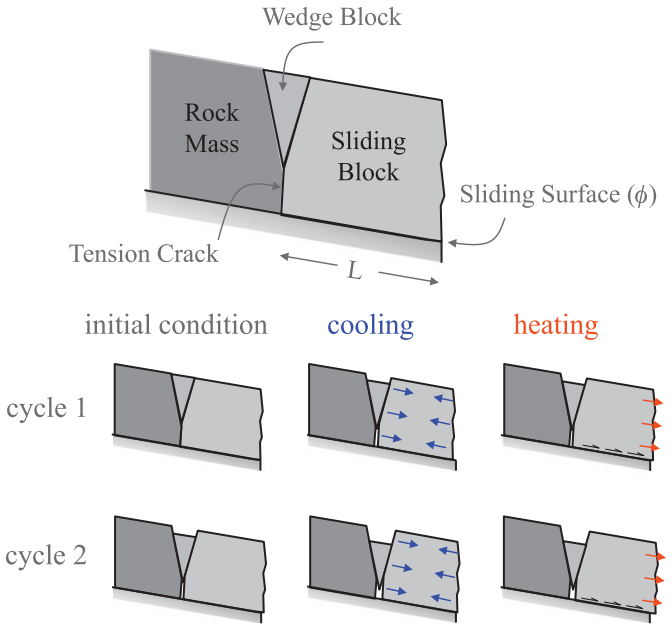

Fig. 7. Cartoon showing the principle elements of the thermally–induced wedging mechanism.

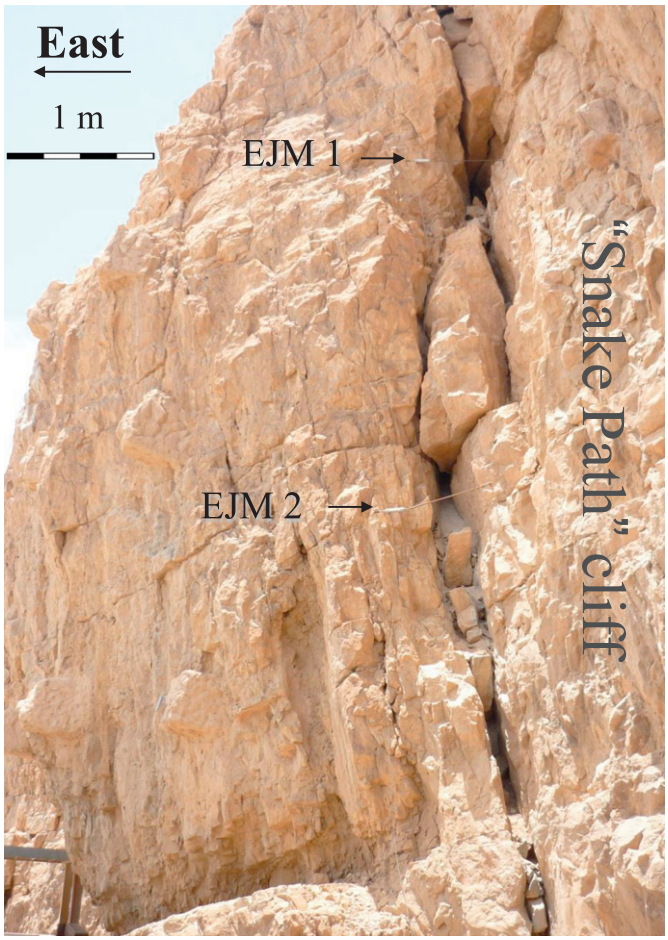

Fig. 8. Wedge blocks in the tension crack of Block 1 at EMS. Block 1 is used for comparison between thermally and dynamically induced sliding mechanisms (see text).

elastic shear response along the sliding interface (δ_j). The unconstrained seasonal thermal expansion (δ_T) of both sides of the tension crack as well as the wedge fragments inside the tension

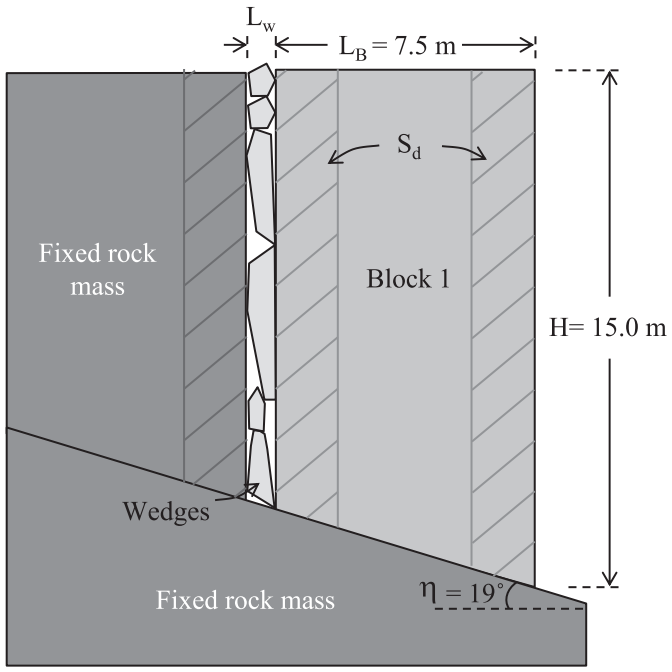

Fig. 9. Exact geometry of Block 1 in the East slope of Masada with rock fragments representing the wedge block in the tension crack. S_d is the skin depth, L_W is the wedge length and L_B is the block length.

crack may be expressed by

$$\delta_T = \alpha \Delta T_p (L_W + 2\beta S_d) \tag{2}$$

where α is the thermal expansion coefficient of the intact rock, ΔT_p is the seasonal temperature change from peak to peak, and β is a coefficient accounting for non-uniform diffusive temperature distribution inside the sliding block and the rock mass ($0<\beta<1$). Note that β is introduced when the skin depth S_d is smaller than the half-length of the rock element.

During a thermal expansion period, uniform compressive stresses develop in the domain leading to an elastic force within the block. Considering Fig. 9, the maximum force parallel to the sliding surface (F_{max}) that the frictional resistance of the sliding plane can sustain is:

$$F_{\max} = \gamma L_B (H - \frac{1}{2} L_B \tan\eta)(\tan\phi\cos\eta - \sin\eta) \tag{3}$$

where γ is the unit weight of the rock ($\gamma=\rho g$), ϕ is the friction angle of the sliding plane, and η is the inclination of the sliding plane. The elastic displacement δ_σ that is developed in the wedge and the block due to F_{max} is

$$\delta_\sigma = \frac{F_{\max}\cos\eta}{HE}(L_W + \frac{L_B}{2}) \tag{4}$$

where E is the modulus of elasticity of the rock material. Only the half-length of the sliding block is considered in the initial element length undergoing contraction since the right boundary of the block (see Fig. 9) is a free surface that does not provide any reaction for F_{max}.

Finally, assuming that the toe of the block (the lower right corner of Block 1 in Fig. 9) is static during the expansion period, the limiting elastic displacement of the interface parallel to the sliding direction δ_j due to F_{max} is

$$\delta_j = \frac{F_{\max}}{k_l L_B}\cos\eta \tag{5}$$

where k_j is the shear stiffness of the sliding interface. During seasonal thermal heating the permanent plastic displacement δ_p

along the sliding surface may be obtained by

$$\delta_p = \begin{cases} \delta_T - \delta_\sigma - \delta_j & if\ (\delta_T - \delta_\sigma - \delta_j) > 0 \\ 0 & else \end{cases} \quad (6)$$

4.2. Physical and mechanical properties of the rock mass in Masada

4.2.1. Experimental determination of thermal conductivity

In order to determine the thermal conductivity of Masada dolomite we use a non-steady-state probe (NSSP) in adherence to ASTM D 5334-00 and D 5930-97 standards. A 2.5 mm diameter hole is drilled at the center of cylindrical dolomite samples with a diameter of 68 mm, a height of 48 mm, and a density of 2600 kg/m^3. A 1.2 mm diameter thermo-resistance needle is used as both heating wire, representing a perfect line source with heat resistance of $R=83.94\ \Omega$/m, and as a temperature sensor at the source (see Fig. 10a). After a short transient period the temperature difference between the source and the measurement point for a constant heating of the needle can be expressed as:

$$\Delta T = A\ln(t) + B \quad (7)$$

where A and B are best-fit parameters that depend upon the heater power Q and the thermal properties of the heated medium. Results of four different tests performed using the NSSP are presented in Fig. 10b on a semi-logarithmic scale. The thermal conductivity λ can be calculated from the linear slope A after the transient period as follows:

$$\lambda = \frac{1}{A}\frac{Q}{4\pi} \quad (8)$$

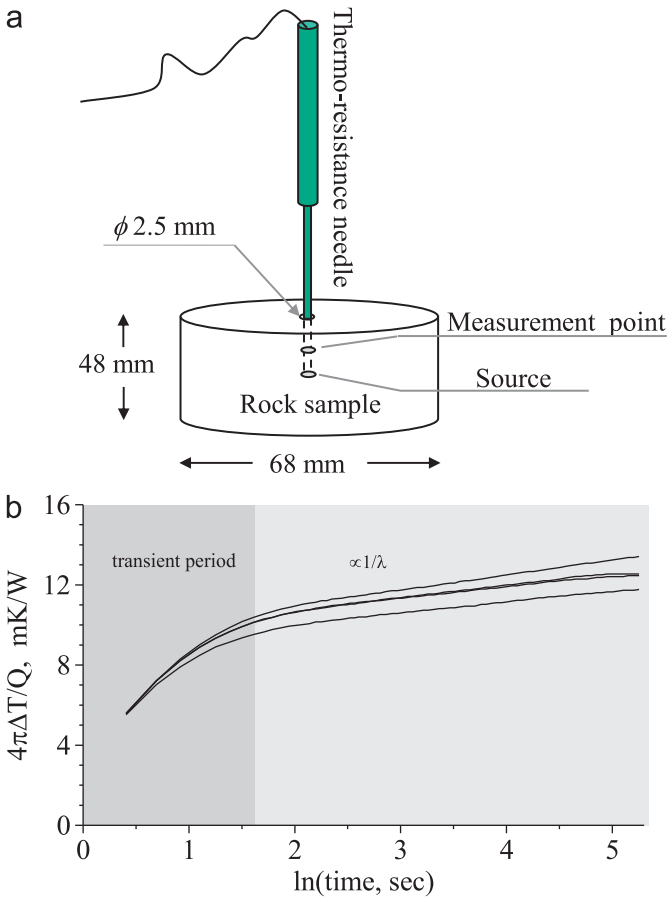

Fig. 10. The NSSP thermal conductivity experiment in the lab: (a) Experimental setting, (b) obtained experimental results.

The average value obtained from four different tests is $\lambda=1.71\pm0.26$ W/mK, a typical value for limestones and dolomites [37]. Using a rock mass density of 2600 kg/m^3 and assuming a typical heat capacity for dolomites of $C_p=810$ J/kgK [37], the estimated thermal skin depth for a seasonal exposure time (Eq. (1)) is $S_d=2.5$ m.

4.2.2. Estimating the thermal expansion coefficient from field measurements

Consider the monitored thermal response of the rock mass at WMS over a single seasonal cycle; note that no permanent displacement of the monitored joints is observed (see Fig. 6b). We believe that this is because the monitored joints in WMS are clean and tight, i.e. because a ratchet mechanism is not possible. We can therefore use these results to compute the thermal expansion coefficient (α) of the Masada rock mass, assuming that the air temperature and the rock temperature across the skin depth are equal during the exposure time. The monitored block length in WMS ($L_B=1.6$ m) is smaller than the estimated skin depth for a seasonal exposure time ($S_d=2.5$ m). Therefore, the joint meter output represents the contraction and expansion of the rock material on both sides of the joint across the thermally affected zone of length L_o, which is assumed to be equal to half of the block length and the equivalent skin depth into the rock mass (see Fig. 11a), namely $L_o=0.5\ L_B+\beta\ S_d$. The thermal expansion coefficient α can be evaluated assuming a linear thermo-elastic response of L_o as follows:

$$\alpha = \frac{d\varepsilon}{dT} = \frac{dL}{L_0}\frac{1}{dT} = \frac{dL}{0.5L_B+\beta S_d}\frac{1}{dT} \quad (9)$$

where $dL=0.14$ mm is the annual joint displacement measured by WJM 2 during an annual temperature amplitude of $dT=9\ ^\circ$C (Fig. 4). We ignore the wedge length in L_o in Eq. (9) because the monitored joint in WMS is extremely tight (see Fig. 2a). The influence of the coefficient β on the computed thermal expansion coefficient is shown in Fig. 11b. Typical α values for dolomites are 6×10^{-6}–$8\times10^{-6}/^\circ$C [38]. We therefore assume a range of values for β between 0.45 and 0.7 in further analysis.

4.2.3. An experimental determination of shear stiffness and strength

Consider Fig. 12, where results of direct shear tests performed on a bedding plane surface from Masada are presented. In this plot, shear stress vs. shear displacement is shown for seven cycles of loading, unloading, and reloading under increasing normal stress from 0.17 to 1.38 MPa, with the normal stress kept constant during each shear sliding segment using closed-loop servo control. In each cycle the sample is sheared forward for a distance of 0.5 mm at a displacement rate of 0.025 mm/s. Inspection of Fig. 12 reveals that a shear displacement of at least 0.09 mm would be required to reach steady state sliding for this particular interface for a sample length of 10 cm. Consequently the shear stiffness for the tested interface k_j is estimated to be 1.0 GPa/m for normal stress of 0.17 MPa. A Mohr–Coulomb failure envelope obtained from reduced data presented in Fig. 12 yield a peak friction angle of 41° for the tested bedding plane surface of Masada dolomite.

4.3. Thermally induced sliding of block 1 in EMS

To check the possibility of obtaining thermally induced sliding in Masada we use the carefully measured geometry of Block 1 in EMS (see Fig. 9) along with the physical properties of the rock mass obtained experimentally both in the laboratory and in the field (see Table 2) as input parameters for the analytical approach summarized in Eqs. (1)–(6) above. The permanent annual thermal plastic displacement thus obtained is plotted in Fig. 13 as a function of wedge length, for non-uniform diffusive distribution

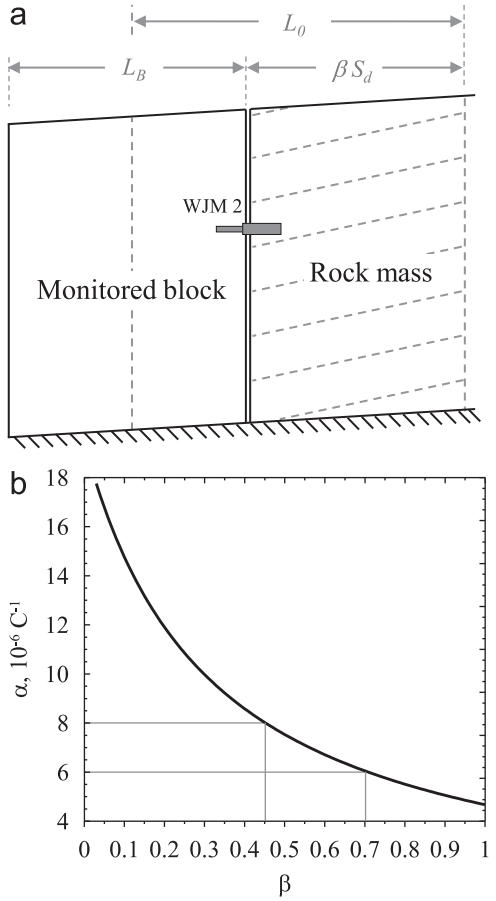

Fig. 11. (a) Definition of length parameters used in Eq. (9), (b) thermal expansion coefficient α as a function of the assumed non-uniform diffusive temperature distribution β. Taking β=0.45 and 0.7 yields $\alpha=8\times10^{-6}$ and 6×10^{-6} 1/°C, respectively.

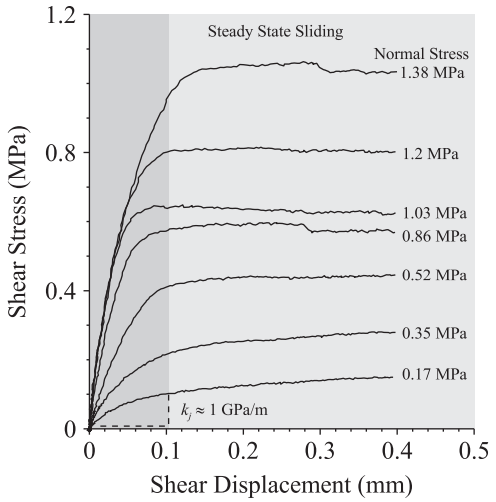

Fig. 12. Results of direct shear tests performed on a natural bedding plane sample from Masada (after [52]). k_j is the shear stiffness of the bedding plane for a normal stress of 0.17 MPa.

coefficients β=0.45 and 0.7. From this analysis we obtain an annual displacement rate for Block 1 ranging from 0.181 to 0.210 mm/year and from 0.238 to 0.260 mm/year for β=0.45 and 0.7, respectively, when increasing the opening of the tension crack from 0 to 200 mm.

Table 2
Mechanical and thermal properties for Block 1 in EMS used for analytical and numerical solutions.

	Symbol	Analytical model Thermal loading	Numerical DDA model Seismic loading
Mechanical properties:			
Elastic Modulus (GPa)	E	40	40
Poisson's Ratio	ν		0.2
Mass density (kg/m^3)	ρ	2600	2600
Friction angles (Deg)	ϕ	41	41
Joint stiffness (GPa/m)	k_j	1	–
Thermal properties and loading:			
Thermal expansion coefficient (C^{-1})	α	$6–8\times10^{-6}$	–
Annual temperature amplitude (°C)	ΔT	9	–
Thermal conductivity (W/(m K))	λ	1.7	–
Specific heat capacity (J/(kg K))	C_p	810 [a]	–
Numerical Parameters:			
Dynamic control parameter		–	1
Number of time steps		–	12000
Time interval (S)	Δt	–	0.005
Assumed max. disp. ratio (m)		–	0.005
Contact stiffness (GN/m)	k	–	500 [b]

[a] Rohsenow et al., 1998 [37].
[b] See text in Section 5.2 for sensitivity analysis procedure.

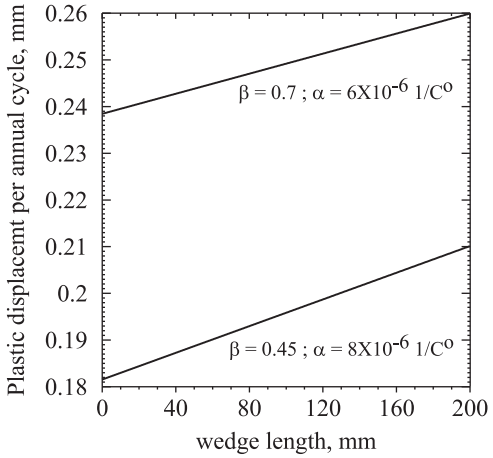

Fig. 13. Thermally induced plastic displacement for a single annual cycle as a function of the wedge length (assuming β=0.45 and 0.7), as obtained using the analytical model of Pasten [35].

5. Seismically induced block displacement

A thermally-induced wedging mechanism that can explain one-directional block displacement in jointed rock masses has been discussed above. This mechanism operates under constant gravitational loading and is driven by cyclic thermal changes. The position of Masada, near a major fault (the Dead Sea rift), calls for a consideration of the possibility of block displacements due to seismic vibrations. We chose Block 1 in the East slope of Masada (EMS) as a case study for testing two different driving mechanisms: thermal vs. seismic, because the geometry of this finite and removable block, the amount of opening of the tension crack, and relevant physical and mechanical parameters for this block are known. Moreover, we have a reasonably well constrained input seismic motion that could be used for dynamic seismic analysis for this block e.g. [39], and the recurrence time of strong earthquakes is available e.g. [40,41].

Masada Mountain is situated along the Dead Sea transform (see Fig. 1a) with moderate seismic activity and an expected maximum

earthquake moment magnitude (M_w) of 7.5 [40,42]. According to the Israeli building code 413 a Peak Ground Acceleration (*PGA*) level of 0.22 g has an excedance probability of 10% at least once within a period of 50 years in Masada area, corresponding to a return period of 475 years. The estimated return period for the Dead Sea region is about 300 years and 4000 years for earthquakes greater than $M_w \geq 6.0$ and $M_w \geq 7.0$, respectively [40,42]. Since instrumental records of strong earthquakes ($M_w > 6.0$) in the Masada region are not available, we use in our analysis a strong event that took place elsewhere in the same tectonic setting, and was recorded instrumentally in a nearby city—the Nuweiba earthquake.

5.1. Seismic input motion for dynamic analysis of block sliding

The $M_w = 7.2$ Nuweiba earthquake occurred on November 22, 1995, in the Gulf of Eilat (Aqaba) with an epicenter near the village of Nuweiba, Egypt (Fig. 1a). The main shock was recorded at a seismological station in the city of Eilat, located 70 km north of the epicenter. The recording station was positioned in a school basement built on a soil cover of 50 m thickness composed of Pleistocene alluvial fan deposits. The recorded acceleration time history therefore represents the site response of the soil layer in Eilat, rather than hard bedrock. A one-dimensional multi-layer model for the soil was utilized by Zaslavsky and Shapira [39] to obtain the rock response by de-convolution, the transfer function based on material and physical parameters determined using both seismic refraction survey data and down-hole velocity measurements in the city of Eilat.

The de-convolution response spectrum thus obtained for the city of Eilat represents a "characteristic" rock response at a distance of 70 km from the epicenter of a $M_w = 7.2$ earthquake in the Dead Sea rift system. To scale this record to the foothills of Masada, we use an empirical attenuation relationship between *PGA*, moment magnitude (M_w), and epicenter distance (R, in km) [43]

$$PGA = \exp[-0.242 + 0.527(M_W - 6) - 0.778\ln\sqrt{R^2 + (5.57)^2} - 0.371\ln(V_s/1396)] \quad (10)$$

where V_s is the average shear-wave velocity of the top 30 m of the ground at the site, assumed here to be 620 m/s. The Nuweiba earthquake record as measured in Eilat and de-convoluted for rock response, is scaled using Eq. (10) for different magnitudes of $M_w = 6.0$, 6.5, 7.0, and 7.5, representing different strong earthquake scenarios in the Dead Sea region. An example of a scaled Nuweiba record corresponding to $M_w = 6.0$ at a distance of 1 km from the epicenter, which yields a *PGA* of 0.275 g, is shown in Fig. 14a. Note that by the scaling procedure the frequency content of the signal remains unchanged. The frequency content is changed however after the convolution procedure according to the site response of the mountain, as discussed below.

Although the Masada site is situated directly on rock, a significant topographic effect was recorded at the site during a geophysical survey in September 1998 [44] and it must be considered in the development of a realistic input motion for dynamic analysis of a block situated at the top of the mountain. The empirical response function for Masada [after 44] is plotted in Fig. 14b where three characteristic modes are found at $f = 1.3$, 3.8, and 6.5 Hz, with frequencies higher than 10 Hz filtered out. This empirical response function for Masada top is applied to the scaled rock response record of Nuweiba to obtain the expected rock response at the top of the mountain. An example of an output using this procedure for a $M_w = 6.0$ event is shown in Fig. 14c. As can be appreciated from the specific examples shown in Figs. 14a and c, the expected *PGA* of 0.275 g at the valley floor (Fig. 14a) is amplified by this procedure to 0.465 g at the mountain top (Fig. 14c). A flowchart summarizing this scaling procedure is shown in Fig. 14d. Note that in this procedure we do not take into account the amplification effects of the rock block itself, as shown by other researchers e.g. [45,46].

By utilizing the attenuation relationship of Boore et al. [43] the expected *PGA* as a function of earthquake epicenter distance from Masada for moment magnitudes 6.0 and 7.5 Dead Sea rift earthquakes is shown in Fig. 15 (dashed lines), representing *PGA* on bedrock at the foothills of Masada. For each curve, the amplified site response at the mountain top (solid lines) is obtained by convolution with the empirical response function for the topographic site effect at Masada as explained above. The *PGA* values of four amplified earthquakes with epicenter at a distance of 1 km from Masada are also shown in Fig. 15 (symbols) for M_w levels of: 6.0, 6.5, 7.0, 7.5. The acceleration time series for these four amplified earthquake records are used as input for numerical analysis of seismic block response using the numerical, discrete-element, Discontinuous Deformation Analysis (DDA) method.

5.2. Numerical procedure using DDA

The DDA method is an implicit discrete element method originally developed by Shi [23] to provide a useful tool for investigating the kinematics of blocky rock masses. DDA models the discontinuous medium as a system of individual deformable blocks that move independently without interpenetration. The method uses standard Finite Element Method (FEM) formulation but here every block is an element and the contacts between blocks are treated using a penalty method for the constraint of no penetration and no tension between the blocks. By the second law of thermodynamics, a mechanical system under loading must move or deform in a direction which produces the minimum total energy of the whole system. For a block system, the total energy consists of the potential energy due to different mechanisms like external loads, block deformation, system constraints, kinetic and strain energy of the blocks and the dissipated irreversible energy. The minimization of the system energy will produce a set of equations of motion for the block system, the same as that used in the FEM. DDA is a dynamic method that utilizes a time-step marching scheme in the solution process so that dynamic block displacement can be modeled in the time domain. The DDA solution guarantees that at the end of every time step there is no penetration and no tension between adjacent blocks by employing an original "open–close" iteration procedure that utilizes a numerical penalty in the form of stiff springs at automatically detected block contacts. The theory of DDA is covered comprehensively by Shi [47]. A review of DDA principles is provided in [48]; more than 100 DDA validation studies are reviewed and discussed in [49]. Based on these validation studies, it is believed that using the DDA method will provide more reliable results for dynamic analysis, provided that proper preliminary sensitivity analyses are performed with respect to the numerical control parameters, most notably the contact spring stiffness, as discussed below.

Results obtained with DDA are sensitive to the choice of both the numerical contact spring stiffness (k) and the time step size (Δt). Therefore, sensitivity analysis has been done to select the most appropriate couple of these numerical control parameters. We use the geometry of Block 1 resting on an inclined plane with no wedge in the tension crack, and subjected to synthetic sinusoidal input loading consisting of constant amplitude and frequency, a problem for which an exact analytical solution exists, known as the Newmark's type analysis [20]. 2D-DDA code verification for this problem is shown by Kamai and Hatzor [50]. Previous code verifications for dynamic cases indicate that the optimal contact spring stiffness in DDA is frequency-dependent. To obtain the optimal k value for our case the two dominant frequencies of the mountain $f_1 = 1.3$ and $f_2 = 3.8$ Hz as obtained

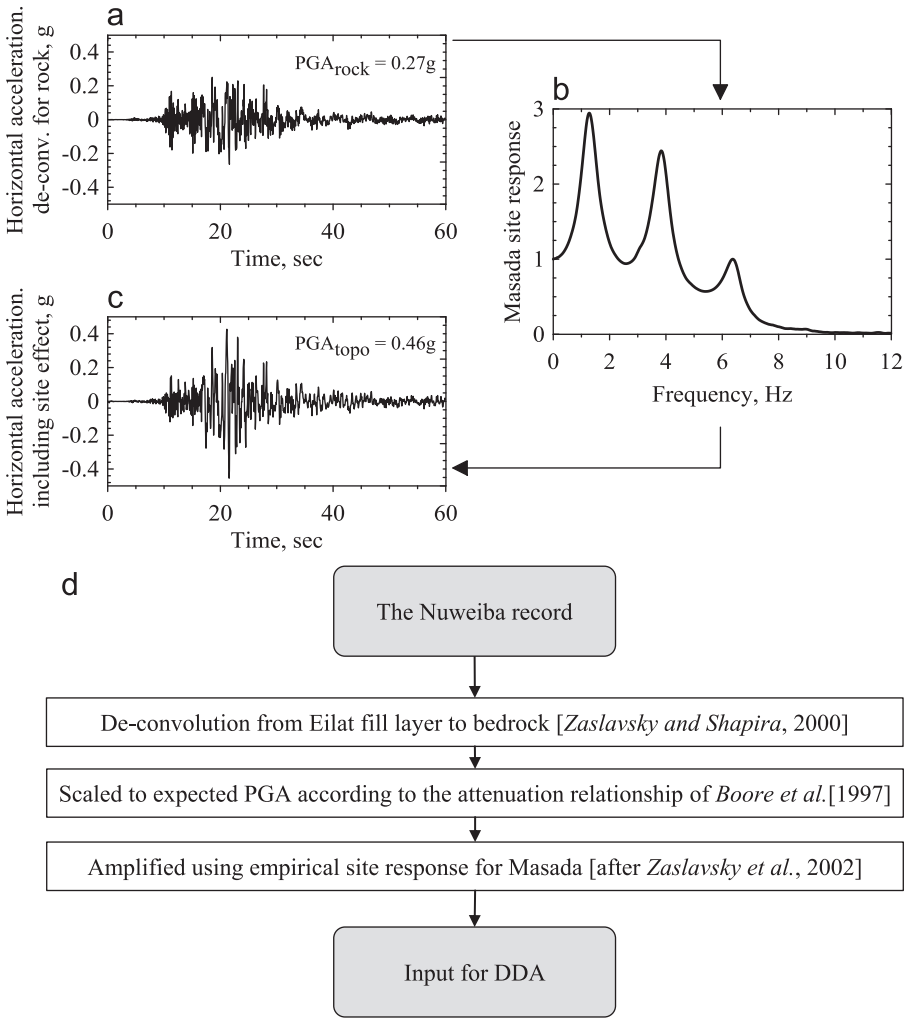

Fig. 14. The input procedure for seismic loading simulations with DDA. (a) The Nuweiba earthquake as recorded in Eilat on a soil layer de-convoluted for bedrock response [39] and scaled to $PGA=0.275$ g, corresponding to a $M_w=6.0$ earthquake at a distance of 1 km from Masada (see Fig. 15), (b) an empirical site response function for Masada [after 44], (c) convoluted time series of the modified Nuweiba record (Fig.14a) to include the empirical site response function for Masada (Fig. 14b), and (d) flowchart summarizing the input procedure.

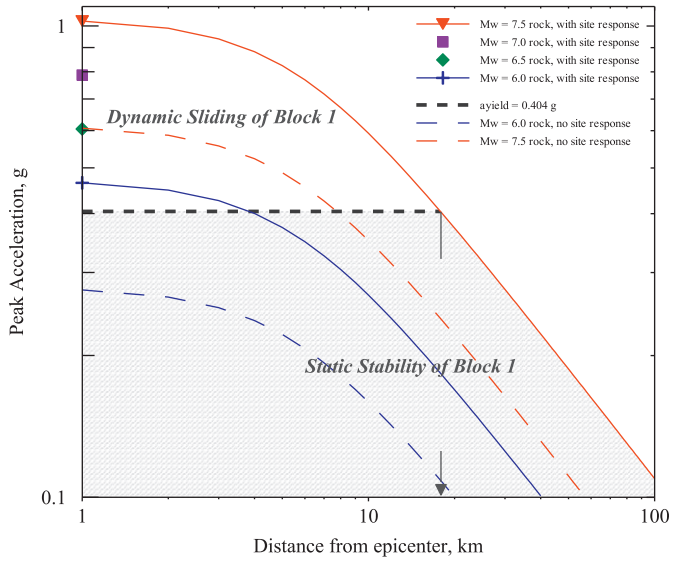

Fig. 15. Assumed attenuation curves for Dead Sea Rift earthquakes [after 43] (dashed lines) with amplification due to topographic site effect at Masada (solid lines and symbols). Shaded region delineates conditions at which seismically-induced sliding of Block 1 at Masada is not possible.

from the topographic site response survey (see Fig. 14b) are used. Eighteen simulations of sinusoidal input functions are performed for each of the dominant frequencies of Masada mountain (f_1 and f_2) with $k=1$, 5, 10, 100, 500, 1000 GN/m, $\Delta t=0.01$, 0.005, 0.002 s, and an arbitrary constant value of 0.5 g for input amplitude.

For each input frequency the optimal numerical parameters are searched based on the lowest relative error between the Newmark analytical solution and the numerical DDA solution at the final position of the block, where the relative error (R_e) for the displacement solutions (D) is defined as

$$R_e = \frac{|D_{analytical} - D_{numerical}|}{|D_{analytical}|} \times 100\% \quad (11)$$

The optimal contact spring stiffness values thus obtained are 10 and 500 GN/m for f_1 and f_2 respectively, and the optimal time step size is 0.005 s for both input frequencies. Using the optimal numerical control parameters a comparison between numerical DDA and analytical results are shown in Fig. 16. To find the optimal contact spring stiffness when the two dominant frequencies are used as input, we multiply each set of relative error values obtained from the numerical computation at each input frequency and search for the lower multiplied value. The obtained optimal contact spring stiffness for the two dominant frequencies of

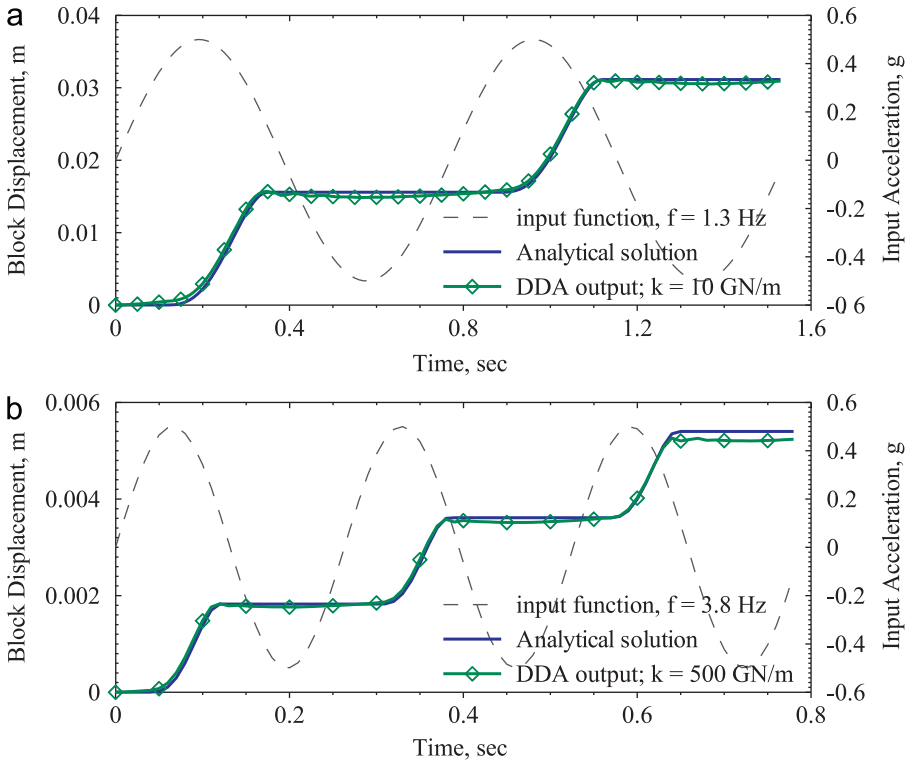

Fig. 16. DDA results vs. analytical (Newmark's) solution for the dynamic displacement of Block 1 when subjected to a sinusoidal input function with 0.5 g amplitude and the two dominant frequencies for Masada (see Fig. 16b): 1.3 Hz (a) and 3.8 Hz (b). (k is the numerical contact spring stiffness used in DDA).

Masada is 500 GN/m. For a list of mechanical and numerical parameters used in the fully dynamic seismic analysis see Table 2.

5.3. Results of seismic analysis for block 1

The horizontal yield acceleration (a_{yield}) for an inclined bedding plane dipping 19° with peak friction angle of 41° as in the case of Block 1 is readily obtained using pseudo-static analysis [21] at a_{yield}=0.404 g. The a_{yield} value thus obtained constrains the epicenter location of the maximum expected earthquake (M_w=7.5) at the Dead Sea rift capable of triggering sliding of Block 1, to a distance of up to 20 km from Masada (Fig. 15).

DDA results for seismic analysis of Block 1 subjected to amplified Nuweiba records corresponding to M_w=6.0, 6.5, 7.0, 7.5 Dead Sea rift earthquakes at an epicenter distance of 1 km from Masada are shown in Fig. 17. For moderate earthquakes ($M_w \leq 6.5$) the block displacement per single event is expected to be lower than 42 mm, whereas for strong earthquakes ($M_w \geq 7.0$) the block is expected to slide more than 447 mm along the inclined bedding plane in a single event. The mapped opening of the tension crack in the field is only 200 mm (see Fig. 17), a value that constrains feasible earthquake scenarios, as discussed below.

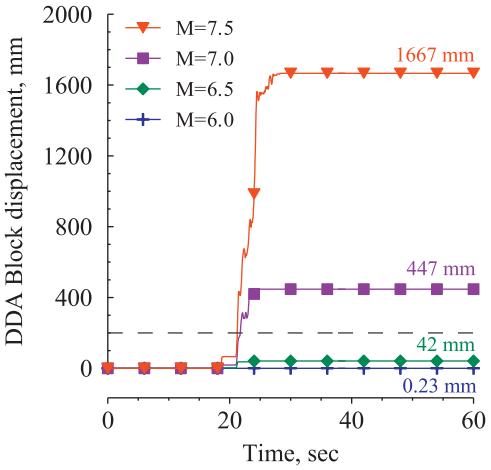

Fig. 17. DDA results for dynamic displacement of Block 1 when subjected to amplified Nuweiba records corresponding to earthquakes with moment magnitude between 6.0 and 7.5 and epicenter distance of 1 km from Masada. Mapped joint opening in the field is plotted (dashed) for reference.

6. Discussion

6.1. Thermoelastic behavior of the Masada rock mass

This work examines the theoretical possibility for thermally induced rock block displacement due to a natural wedging mechanism, where the key elements are the intact rock mass, the tension crack, the wedge fragments, the sliding block, and the sliding surface (see Fig. 7). Although the geometry of the model discussed in this paper is well defined, we argue that the presented mechanism may lead to permanent sliding block displacements wherever wedging blocks are formed in tension cracks, as also suggested by Watson et al. [13]. Moreover, it is shown that thermally induced sliding can also occur on shallow dipping planes, not typically considered unstable.

The monitoring station at West Masada (Fig. 2) is installed on a block that is separated from the rock slope by clean and tight joints with no wedge fragments. We assume that for this reason, no permanent displacement has been recorded during the monitoring period in the West slope. On the other hand, we assume that the wedge fragments inside the tension crack of Block 1 in the East slope (Fig. 8) can trigger the wedging mechanism conceptually illustrated in Fig. 7. Since cable bolts were installed during the summer of 1998 to anchor Block 1 to the cliff, in connection with a comprehensive

slope reinforcement campaign, no evidence for permanent displacement since then is available. We therefore utilize the results obtained from the monitoring system at WMS to evaluate the thermal expansion coefficient α of the Masada rock mass, for the analysis of thermally induced displacement of Block 1 in EMS.

Thermal conductivity measurements performed on a sample from Masada (Fig. 10) enable us to estimate the skin depth for the Masada rock mass for a seasonal exposure time at $S_d \approx 2.5$ m, assuming homogeneous, one-dimensional, temperature distribution within the rock element. In reality, however, the temperature distribution within the rock mass is not homogenous and the parameter β for non-uniform diffusive temperature distribution must be considered. A range of values of $0.45 < \beta < 0.7$ is used here assuming a typical range for the thermal expansion coefficient α for the Masada rock mass from 6×10^{-6} to $8 \times 10^{-6}/^{\circ}$C [38]. This set of parameters (for α and β) are used to calculate the permanent thermally induced annual plastic displacement using the analytical model suggested by Pasten [35] in Eqs. (2)–(6).

It is important to note that the parameter β depends on the rock mass geometry and on the tension crack aperture. In the West station, the data from which the parameter β is based on, the tension crack is very tight, and we therefore expect a non-uniform thermal distribution within the rock mass and consequently a relatively thin thermal skin depth. On the other hand, the tension crack behind Block 1 in EMS is relatively wide and the block is clearly separated from the rock slope (Figs. 3a and 8); it is therefore expected that the block responds more uniformly and therefore the actual value of parameter β may be higher than assumed here.

6.2. Block displacement rate under thermal and seismic loading

Block 1 is used to study displacement rates under thermal loading on one hand and seismic loading on the other hand. The geometry of the block is completely known, as well as the mechanical and physical parameters of the intact block material and the shear strength and shear stiffness of the sliding surface. Moreover, the magnitude of opening in the tension crack is readily measurable in the field and amounts to 200 mm. An inclination of 19° and a friction angle of 41° for the sliding plane are assumed in the analysis, based on field and laboratory measurements.

Analytical results (Fig. 13) show that the thermally induced sliding rate of Block 1 ranges from 0.181 to 0.210 mm/year for β=0.45, and from 0.238 to 0.260 mm/year, for β=0.7. The sliding rate increases with time because the increased aperture of the tension leads to increased wedge block length L_W. This is true as long as the assumed skin depth is larger than the wedge length ($S_d > L_W$) and provided that a continuous supply of detritus material is made available from higher segments of the rock slope above the tension crack. Furthermore, it is assumed that the crushing strength of the detritus material is sufficiently high so as to sustain the compressive force F_{max} that develops in the block system during the expansion periods.

To obtain the displacement rate under seismic loading we must first make some assumptions regarding the recurrence probability of Dead Sea rift earthquakes. Based on paleo-seismic, historical, and instrumental records, the return period for moderate (M_w=6.5) and strong (M_w=7.0) Dead Sea rift earthquakes is estimated to be 1100 and 4000 years, respectively [40,42]. Consider Fig. 17 where results of dynamic numerical analyses for the displacement of Block 1 under amplified Dead Sea rift M_w=6.0–7.5 earthquakes with epicenter at a distance of 1 km from Masada are presented. From this chart equivalent displacement rates of 0.04 mm/year and 0.11 mm/year may be deduced for moderate (M_w=6.5) and strong (M_w=7.0) Dead Sea rift earthquakes. These rates clearly provide an upper bound because they apply to an earthquake epicenter at a distance of only 1 km from Masada; with increasing epicenter distance up to 20 km from Masada (see Fig. 15), the expected displacement of Block 1 under a single episode, and consequently the deduced displacement rates, would naturally be smaller.

The displacement rates of Block 1 under moderate Dead Sea rift earthquakes at an epicenter distance of 1 km from Masada, along with the rate deduced from the thermal mechanism, are plotted in Fig. 18. Inspection of Fig. 18 clearly reveals that the thermal mechanism is more dominant than the seismic loading mechanism when each is considered individually.

6.3. Paleo-seismic implications

The total mapped opening of the tension crack in Block 1 (200 mm) imposes some constraints on possible paleo-seismic scenarios at Masada. Consider for example strong Dead Sea rift earthquakes ($M_w \geq 7.0$) with an epicenter 1 km from Masada, the amount of sliding in a single episode is expected to be greater than 447 mm (see Fig. 17); therefore Block 1, in its current configuration, could never have experienced a $M_w \geq 7.0$ earthquake at such close proximity to Masada. However, a single $6.5 < M_w < 7.0$ event at the foothills of Masada, or a stronger event ($M_w > 7.0$) at a distance of up to 20 km from the site (see Fig. 15), could open the tension crack by the observed 200 mm at once. Therefore, we cannot rule out these last two scenarios from our field and analytical data.

We have established that under thermal loading the mapped opening of 200 mm could have been attained over a period of ca. 1000 years assuming climatic conditions have remained more or less the same over this time period. To examine if this opening could have been triggered by seismic vibrations it would be instructive to search the historic regional earthquake catalog and seek an $M_w > 6.5$ event at a distance of up to 20 km from Masada during that time window. The historical earthquake catalog in the Eastern Mediterranean region is based on a long and well-documented historical record and a wealth of archaeo-seismological information. Based on the historical earthquake catalog compiled by Ben-Menahem [51], the earthquakes of May 362 and of May 1834, both located at the Eastern Lisan peninsula (for location see Fig. 1a) with estimated local magnitude of 6.7, may have been possible candidates for triggering the observed displacements in Block 1, however the low accuracy of the assumed magnitude and location precludes any robust conclusions.

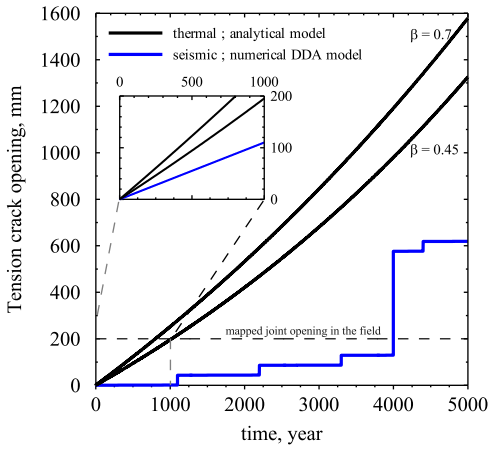

Fig. 18. Comparison between thermally and seismically induced displacement rates for Block 1. Thermal displacement rate is calculated assuming β=0.45 and 0.7. Seismic displacement rate is obtained by summation of earthquake magnitudes 6.0 to 7.0 with epicenter located 1 km from Masada based on the seismicity of the region. The seismic rates in the zoom-in box are for the long term seismicity (5000 years).

7. Summary and conclusions

We present in this paper the possibility for a thermally induced wedging mechanism for rock slopes using the monitored rock blocks at Masada Mountain, Israel, as a case study. The thermal mechanism involves the rock mass, a wedge filled tension crack, a sliding block, and a sliding interface with the rock mass. We show that for the dolomites of Masada the seasonal temperature amplitude is sufficient to induce permanent plastic displacement of rock blocks via a wedging–ratcheting mechanism, although the blocks are situated on relatively shallow dipping planes

Since Masada is situated on the margins of a seismically active rift, we use numerical discrete element analysis to compute the seismically induced displacement of the same block we use to demonstrate the thermal loading mechanism and find that for the assumed seismicity of the region, the 200 mm displacement of the studied block is more likely to have been thermally, rather than seismically, induced.

We conclude that the thermally induced sliding mechanism should be considered when quantitatively assessing surface erosion or rock slopes with thermal and mechanical properties that permit this failure mechanism to take place. This mechanism may explain rock failure episodes occurring more frequently than is generally assumed or explained.

Acknowledgment

Financial support from the US–Israel Binational Science Foundation (BSF) through contract no. 2004122 is gratefully acknowledged. Ulrich Corsmeier from Karlsruhe Institute of Technology is thanked for sharing his data from the West Masada metrological station. The Israel Nature and Parks Authority (INPA) and Eitan Campbell from Masada National Park are thanked for supplying the high quality photographs of the West slope of the Mountain and for assistance in the installation of our monitoring devices. Valentin Gischig is thanked for his critical review, which has greatly improved the quality of this paper.

References

[1] Rodriguez CE, Bommer JJ, Chandler RJ. Earthquake-induced landslides: 1980–1997. Soil Dynam Earthq Eng 1999;18:325–46.
[2] Yagoda-Biran G, Hatzor YH, Amit R, Katz O. Constraining regional paleo peak ground acceleration from back analysis of prehistoric landslides: Example from Sea of Galilee, Dead Sea transform. Tectonophysics 2010;490:81–92.
[3] Iverson RM. Landslide triggering by rain infiltration. Water Resour Res 2000;36:1897–910.
[4] Veveakis E, Vardoulakis I, Di Toro G. Thermoporomechanics of creeping landslides: The 1963 Vaiont slide, northern Italy. J Geophys Res Earth Surf 2007; 112:21.
[5] Matsuoka N. Frost weathering and rockwall erosion in the southeastern Swiss Alps: Long-term (1994–2006) observations. Geomorphology 2008;99:353–68.
[6] Murton JB, Peterson R, Ozouf JC. Bedrock fracture by ice segregation in cold regions. Science 2006;314:1127–9.
[7] Williams PJ. Permafrost and climate change—geotechnical implications. Phil Trans Roy Soc Lon Ser A Math Phys Eng Sci 1995;352:347–58.
[8] Gischig VS, Moore JR, Evans KF, Amann F, Loew S. Thermomechanical forcing of deep rock slope deformation: 1. Conceptual study of a simplified slope. J Geophys Res Earth Surf 2011;116:F04010.
[9] Gischig VS, Moore JR, Evans KF, Amann F, Loew S. Thermomechanical forcing of deep rock slope deformation: 2. The Randa rock slope instability. J Geophy Res Earth Surf 2011;116:F04011.
[10] Gunzburger Y, Merrien-Soukatchoff V, Guglielmi Y. Influence of daily surface temperature fluctuations on rock slope stability: case study of the Rochers de Valabres slope (France). Int J Rock Mech Min Sci 2005;42:331–49.
[11] Hatzor YH. Keyblock stability in seismically active rock slopes—Snake Path cliff, Masada. J Geotech Geoenviron Eng 2003;129:697–710.
[12] Mufundirwa A, Fujii Y, Kodama N, Kodama J. Analysis of natural rock slope deformations under temperature variation: A case from a cool temperate region in Japan. Cold Reg Sci Tech 2011;65:488–500.
[13] Watson A, Moore D, Stewart T. Temperature influence on rock slope movements at Checkerboard Creek. In: Proceedings of the 9th international symposium on landslides. Rio de Janeiro, Brazil; 2004. p. 6.
[14] Vicko J, Greif V, Grof V, Jezny M, Petro L, Brcek M. Rock displacement and thermal expansion study at historic heritage sites in Slovakia. Environ Geol 2009;58:1727–40.
[15] Greif V, Sassa K, Fukuoka H. Failure mechanism in an extremely slow rock slide at Bitchu-Matsuyama castle site (Japan). Landslides 2006;3:22–38.
[16] Hatzor YH, Talesnick M, Tsesarsky M. Continuous and discontinuous stability analysis of the bell-shaped caverns at Bet Guvrin, Israel. Int J Rock Mech Min Sci 2002;39:867–86.
[17] Vargas JE, Velloso R, Chávez L, Gusmão L, Amaral C. On the effect of thermally induced stresses in failures of some rock slopes in Rio de Janeiro, Brazil. Rock Mech Rock Eng 2013;46:123–34.
[18] Goodman R, Shi G. Block theory and its application to rock engineering. Englewood Cliffs, NJ: Prentice-Hall; 1985.
[19] Brune JN. Precarious-rock constraints on ground motion from historic and recent earthquakes in southern California. Bull Seismol Soc Amer 2002;92:2602–11.
[20] Newmark NM. Effects of earthquakes on dams embankments. Geotechnique 1965;15:139–60.
[21] Goodman RE, Seed HB. Earthquake induced displacements in sands and embankments. J Soil Mech Found Div ASCE 1966;92(SM2):125–46.
[22] Cundall PA. Strack ODL. Discrete numerical-model for granular assemblies. Geotechnique 1979;29:47–65.
[23] Shi G. Discontinuous deformation analysis—a new numerical method for the statics and dynamics of block system. PhD thesis. University of California, Berkeley; 1988.
[24] Bouchon M, Barker JS. Seismic response of a hill: The example of Tarzana, California. Bull Seismol Soc Amer 1996;86:66–72.
[25] ChavezGarcia FJ, Sanchez LR, Hatzfeld D. Topographic site effects and HVSR. A comparison between observations and theory. Bull Seismol Soc Amer 1996;86:1559–73.
[26] Geli L, Bard PY, Jullien B. The effect of topography on earthquake ground motion—a review and new results. Bull Seismol Soc Amer 1988;78:42–63.
[27] Zaslavsky Y, Shapira A. Experimental study of topographic amplification using the Israel Seismic Network. J Earthq Eng 2000;4:43–65.
[28] Ashford SA, Sitar N, Lysmer J, Deng N. Topographic effects on the seismic response of steep slopes. Bull Seismol Soc Amer 1997;87:701–9.
[29] Sagy A, Reches Z, Agnon A. Hierarchic three-dimensional structure and slip partitioning in the western Dead Sea pull-apart. Tectonics 2003;22:17.
[30] Israel Meteorological Service. Climate information. ⟨http://www.ims.gov.il/IMSEng/CLIMATE⟩. 2011.
[31] Corsmeier U. Meteorological Observation and Assimilation of the Atmosphere on Long term (Dead Sea, Israel). ⟨http://www.imk-tro.kit.edu/english/4520_3690.php⟩. 2006.
[32] Schmitz S. Untersuchung thermisch induzierter Hang- und Talwindsysteme am Toten Meer und deren Kopplung an größere Skalen. MSc. thesis. Karlsruhe Institute for Technology, Karlsruhe, Germay; 2009.
[33] SIM STRUMENTI. Products. ⟨http://www.simstrumenti.com/en/products.html⟩. 2009.
[34] Whipple KX, Hancock GS, Anderson RS. River incision into bedrock: Mechanics and relative efficacy of plucking, abrasion, and cavitation. Geol Soc Amer Bull 2000;112:490–503.
[35] Pasten C. Repetitive Loadings in Geomaterials. PhD thesis. Georgia Institute of Technology, Atlanta, GA; 2012.
[36] Carslaw HS, Jaeger JC. Conduction of heat in solids. 2nd ed. Oxford, London: Clarendon Press; 1959.
[37] Rohsenow WM, Hartnett JP, Cho YI. Handbook of heat transfer. 3rd ed. New York: McGraw-Hill; 1998.
[38] Franklin JA, Dusseault MB. Rock engineering. New York: McGraw-Hill; 1988.
[39] Zaslavsky Y, Shapira A. Questioning nonlinear effects in Eilat during MW= 7.1 Gulf of Aqaba earthquake. In: Proceedings of XXVII General Assembly of the European Seismological Commission (ESC), Lisbon, Portugal. September 10–15 2000. p. 343-7.
[40] Begin ZB. Destructive Earthquakes in the Jordan Valley and the Dead Sea - their Recurrence Intervals and the Probability of their Occurrence. Geological Survey of Israel, Report No. 12/05; 2005.
[41] Hamiel Y, Amit R, Begin ZB, Marco S, Katz O, Salamon A, et al. The Seismicity along the Dead Sea Fault during the Last 60,000 Years. Bull Seismol Soc Amer 2009;99:2020–6.
[42] Shapira A, Hofstetter R, Abdallah AQF, Dabbeek J, Hays W. Earthquake hazard assessments for building codes—final report. Geophysical Institute of Israel; 2007. p. 88.
[43] Boore DM, Joyner WB, Fumal TE. Equations for estimating horizontal response spectra and peak acceleration from western North American earthquakes: a summary of recent work. Seismol Res Letts 1997;68:26.
[44] Zaslavsky Y, Shapira A, Arzi AA. Earthquake site response on hard rock-empirical study. In: Hatzor YH, editor. Stability of rock structures: Proceedings of the Fifth International Conference of Analysis of Discontinuous Deformation. Lisse: Balkema Publishers; 2002. p. 133–44.
[45] Burjanek J, Gassner-Stamm G, Poggi V, Moore JR, Fah D. Ambient vibration analysis of an unstable mountain slope. Geophys J Int 2010;180:820–8.
[46] Burjanek J, Moore JR, Molina FXY, Fah D. Instrumental evidence of normal mode rock slope vibration. Geophys J Int 2012;188:559–69.

[47] Shi GH. Block system modeling by discontinuous deformation analysis. Southampton, UK: Computational Mechanics Publications; 1993.
[48] Jing L. A review of techniques, advances and outstanding issues in numerical modelling for rock mechanics and rock engineering. Int J Rock Mech Min Sci 2003;40:283–353.
[49] MacLaughlin MM, Doolin DM. Review of validation of the discontinuous deformation analysis (DDA) method. Int J Numer Anal Meth Geomech 2006;30:271–305.
[50] Kamai R, Hatzor YH. Numerical analysis of block stone displacements in ancient masonry structures: A new method to estimate historic ground motions. Int J Numer Anal Meth Geomech 2008;32:1321–40.
[51] Ben-Menahem A. Four thousand years of seismicity along the Dead Sea rift. J Geophys Res 1991;96:20195–216.
[52] Hatzor YH, Arzi AA, Zaslavsky Y, Shapira A. Dynamic stability analysis of jointed rock slopes using the DDA method: King Herod's Palace, Masada, Israel. Int J Rock Mech Min Sci 2004;41:813–32.